Title
Transport of intensity phase imaging in the presence of curl effects induced by strongly absorbing photomasks.

Journal
Applied Optics, 53(34)

ISSN
0003-6935

Authors
Shanker, Aamod
Tian, Lei
Sczyrba, Martin
et al.

Publication Date
2014-12-01

DOI
10.1364/ao.53.0000j1

Peer reviewed

Transport of intensity phase imaging in the presence of curl effects induced by strongly absorbing photomasks

Aamod Shanker,[1] Lei Tian,[1] Martin Sczyrba,[2] Brid Connolly,[3]
Andrew Neureuther,[1] and Laura Waller[1,*]

[1]Department of Electrical Engineering and Computer Sciences, University of California, Berkeley, California, USA

[2]AMTC, Raehnitzer Allee 9, 01109 Dresden, Germany

[3]Toppan Photomasks Dresden, Raehnitzer Allee 9, 01109 Dresden, Germany

*Corresponding author: lwaller@alum.mit.edu

Received 9 July 2014; revised 18 September 2014; accepted 19 September 2014;
posted 19 September 2014 (Doc. ID 216606); published 23 October 2014

We report theoretical and experimental results for imaging of electromagnetic phase edge effects in lithography photomasks. Our method starts from the transport of intensity equation (TIE), which solves for phase from through-focus intensity images. Traditional TIE algorithms make an implicit assumption that the underlying in-plane power flow is curl-free. Motivated by our current study, we describe a practical situation in which this assumption breaks down. Strong absorption gradients in mask features interact with phase edges to contribute a curl to the in-plane Poynting vector, causing severe artifacts in the phase recovered. We derive how curl effects are coupled into intensity measurements and propose an iterative algorithm that not only corrects the artifacts, but also recovers missing curl components.

OCIS codes: (100.5070) Phase retrieval; (110.3960) Microlithography; (080.4865) Optical vortices.
http://dx.doi.org/10.1364/AO.53.0000J1

1. Introduction

The transport of intensity equation (TIE) describes how phase can be recovered from intensity images captured at different focus positions. Its experimental simplicity makes it amenable to existing microscopes in optical [1–6], x-ray [7,8], and electron [9–11] imaging. Subwavelength phase accuracy and real-time processing [12] are routinely achieved and errors can be reduced with multiple images [5,13,14]. One particularly convenient advantage of the TIE method is that it is fairly robust under partially coherent illumination [15,16], making it suitable for lithography aerial imaging tools, which we use here.

1559-128X/14/3400J1-06$15.00/0

The TIE is directly derived from the paraxial wave equation to relate intensity variations over small defocus distances to gradients of phase as light propagates [1]. Being a partial differential equation, solving the TIE involves inverting the equation to recover phase. The traditional TIE solver has an implicit assumption that any curl component in the power flow is not captured in the intensity data. Thus, the TIE is thought to only recover the "scalar" part of the phase and fails for the "rotational" component [15,17]. In fact, the rotational (curl) component does affect the through-focus intensity and, therefore, causes phase artifacts in the traditional TIE solver. A standard example of a wave field with a curl is a phase vortex. This class of curl components has been studied in detail, and it was shown empirically that phase vortices can be recovered by either an iterative algorithm that uses many images through-focus [18] or by modifying the traditional TIE solver [19], assuming small intensity gradients [20].

Here, we discuss a different class of curl effects (distinct from phase vortices) that arise in our application and in any situation where phase gradients are not collinear with intensity gradients. This case has been studied theoretically [21,22], but a solution to the phase recovery problem was not presented. Here, we study the nonphysical phase recovery artifacts resulting from curl components induced by strong absorption. We then propose an iterative wrapper for the traditional TIE solver that corrects such errors to produce a more accurate phase result. This method was first described in [23,24] and later appeared in [25]. We further derive how the curl component is coupled into the intensity measurements, and show that our proposed method also recovers part of the missing curl.

This work is motivated by our studies of electromagnetic phase edges in optical lithography masks [23,24]. Unlike many other applications, photomasks are designed specifically to have strong absorption. An ideal mask would be infinitesimally thin, with no phase variations. Since material constraints mean that real-world masks are thick relative to the size of the feature, the optical field incurs unwanted 3D diffraction effects as it passes through the mask, termed “electromagnetic edge effects” [26–28] (Fig. 1). The result is that the field exiting the mask has added complex-field variations near the feature edges. The real component is easily measured as a line edge placement bias, but the phase component produces an asymmetrical, feature-dependent edge placement change through-focus, which is difficult to measure. As node sizes shrink, these undesired phase effects become more prominent and also more problematic, reducing the process window.

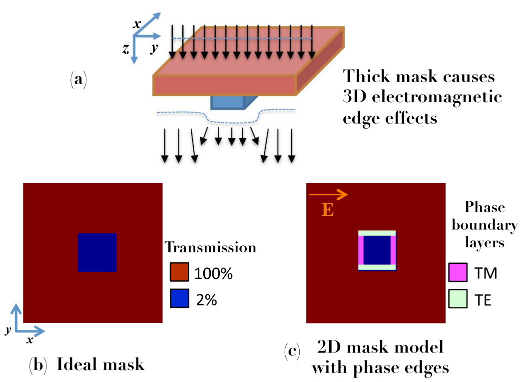

Fig. 1. Photolithography masks incur polarization-dependent electromagnetic edge effects. (a) Because the mask is relatively thick, the electric field accumulates an unwanted phase delay at the feature edges, due to diffraction. (b) An ideal mask has only absorption variations. (c) Phase edge effects can be modeled by phase strips at the feature edges, depending on polarization [26–28].

Mask designers often account for electromagnetic effects using an equivalent thin-mask model, which replaces the complicated 3D effects with a 2D complex field at the exit plane of the mask. For example, boundary layer models represent the added phase effects with quadrature (90 deg) phase strips along the feature edges [26–28], where the width of the strip depends on the mask shape and material. The phase edges are also polarization-dependent, being much stronger in the direction perpendicular to the electric field, so separate boundary layers must be used for each polarization.

In this work, we aim to physically measure phase edge effects using the TIE method in an aerial inspection tool. However, phase variations always occur at the edges of features, where intensity changes rapidly. Since the gradients of the intensity and phase are not collinear, significant curl components result near the feature corners, and we must correct the artifacts in order to recover the phase accurately.

2. Transport of Intensity Equation Solvers and Curl Effects

First, we describe the traditional TIE solver and derive how an absorption-induced curl can produce errors in the phase result. For a 2D complex object $\sqrt{I}e^{i\phi}$ with intensity I and phase ϕ, the TIE describes the change of axial intensity as a divergence of the in-plane power flow [1,2],

$$\frac{\mathrm{d}I}{\mathrm{d}z} = -\frac{\lambda}{2\pi}\vec{\nabla}\cdot I\vec{\nabla}\phi, \tag{1}$$

where λ is wavelength, $\vec{\nabla}$ is the lateral gradient, and z is the defocus distance. Thus, one can solve for phase after estimating the intensity derivative $\mathrm{d}I/\mathrm{d}z$ from two or more intensity images at different z.

Since $\vec{\nabla}$, I, and ϕ are in-plane, $I\vec{\nabla}\phi$ is the in-plane Poynting vector [15]. To solve Eq. (1), Teague's solver [1] defines an auxiliary variable ψ such that $\vec{I}\nabla\phi = \vec{\nabla}\psi$, which converts the TIE into a Poisson equation,

$$\frac{\mathrm{d}I}{\mathrm{d}z} = -\frac{\lambda}{2\pi}\nabla^2\psi. \tag{2}$$

Equation (2) can use any Poisson solver (e.g., in the Fourier domain [29]) to solve for the auxiliary variable ψ. Substituting this value back into its relation with phase gives $\vec{\nabla}\phi = \vec{\nabla}\psi/I$, and taking another divergence yields a Poisson equation in phase,

$$\vec{\nabla}\cdot(\vec{\nabla}\psi/I) = \nabla^2\phi, \tag{3}$$

from which a second Poisson solver can recover the final phase $\phi(x,y)$ to within an unimportant constant offset. This two-step solution is required for objects with nonuniform absorption. For the case of constant intensity (e.g., a pure phase object), $I(x,y) = I_0$, and the phase is recovered directly after solving the first Poisson equation, $\phi = \psi / I_0$.

It has been noted [21,22] that substituting the Poynting vector with the gradient of a scalar field [to obtain Eq. (2)] makes the implicit assumption that the Poynting vector is curl-free, requiring collinearity of the phase and intensity gradients:

$$\vec{\nabla} \times (I\vec{\nabla}\phi) = \vec{\nabla} I \times \vec{\nabla}\phi = 0. \tag{4}$$

As described previously, photomasks have both strong absorption and phase at the edges of features, resulting in a significant curl component (i.e., noncollinear phase and intensity gradients). This is illustrated in Fig. 2 for a simulated OMOG (Opaque MoSi on Silica)-type mask with a 2% transmitting block on a clear background. To model electromagnetic edge effects for horizontally polarized illumination, we add a boundary layer of width 20 nm with a 90 deg quadrature phase along the vertical direction. In this simulation, parameters have been chosen to match those of our experiment, described later. We use a deep UV wavelength $\lambda = 193$ nm, NA 1.35 at the wafer (0.3375 at the mask), and illumination coherence $\sigma = 0.3$. Since the phase strips are much smaller than the resolution of the optical system, they become blurred and result in smaller peak phase values. Here, we directly observe that the gradients of the intensity and phase are noncollinear at the corners, leading to a non-negligible curl for the in-plane Poynting vector, $\vec{\nabla} I \times \vec{\nabla}\phi \neq 0$. The curl components for this simulated mask are shown in Fig. 2, along with the phase recovered by Teague's solver (using the Poisson solver in [29,30]). This phase result incurs a significant error, due to curl effects.

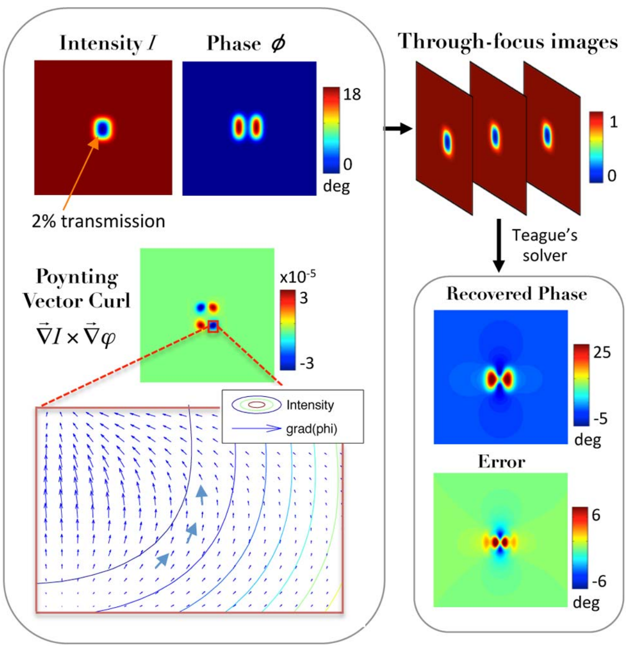

Fig. 2. (Left) Simulation of a 240 nm square absorbing feature on a photomask with phase edges added along the vertical sides, causing a nonzero curl in the Poynting vector near the feature corners, where the phase gradient is tangential to intensity contours. (Right) When through-focus images are simulated for this complex field and are used as input to the traditional TIE solver, the phase recovered suffers serious errors due to the curl effects.

To calculate the phase error due to the missing curl, consider the Helmholtz decomposition of the Poynting vector, with curl-free and divergence-free source terms [15],

$$I\vec{\nabla}\phi = \vec{\nabla}\psi + \vec{\nabla} \times \vec{\mathbf{A}}_1, \tag{5}$$

where ψ and $\vec{\mathbf{A}}_1$ are the scalar and vector potentials of the power flow, respectively. Since the TIE describes the divergence of the Poynting vector, the first Poisson equation [Eq. (2)] of Teague's solution is uniquely and exactly solved for the scalar potential ψ, given appropriate boundary conditions. In the presence of a vector potential for the Poynting vector [Eq. (5)], however, the second Poisson equation in Teague's solution [Eq. (3)] has an extra term due to the curl,

$$\vec{\nabla} \cdot \frac{\vec{\nabla}\psi}{I} + \vec{\nabla} \cdot \frac{\vec{\nabla} \times \mathbf{A}_1}{I} = \nabla^2\phi, \tag{6}$$

$$\Rightarrow \nabla^2\phi_{\mathrm{TIE}} + \nabla^2\phi_{\mathrm{res}} = \nabla^2\phi, \tag{7}$$

where ϕ_{TIE} is the phase returned by Teague's solver and ϕ_{res} is the residual error that occurs due to the curl component, shown in Fig. 2 to create a severe saddle-shaped artifact for a square feature.

3. Recovering Curl by Iterative Transport of Intensity Equation

Next, we describe our algorithm and prove analytically that the curl components of the power flow are not entirely lost in through-focus measurements, and can thus be recovered computationally. We demonstrate this on the simulated photomask described above, as well as in experimental measurements, showing its efficacy in the presence of strong absorption.

Our algorithm iterates back and forth through Teague's solver, estimating both the phase and the curl component at each step. In the first step, we obtain an initial phase estimate using Teague's method, ϕ_{TIE}, then plug it back into the TIE to estimate the axial intensity derivative that would have been produced by ϕ_{TIE},

$$\left.\frac{\mathrm{d}I}{\mathrm{d}z}\right|_{\mathrm{est}} = -\frac{\lambda}{2\pi}\vec{\nabla} \cdot I\vec{\nabla}\phi_{\mathrm{TIE}}. \tag{8}$$

The residual intensity derivative is then obtained by calculating the difference between the estimated and measured intensity derivatives,

$$\left.\frac{\mathrm{d}I}{\mathrm{d}z}\right|_{\mathrm{res}} = \frac{\mathrm{d}I}{\mathrm{d}z} - \left.\frac{\mathrm{d}I}{\mathrm{d}z}\right|_{\mathrm{est}}, \tag{9}$$

and is expected to be 0 in the absence of curl, notwithstanding numerical errors and noise. The residual intensity derivative is then used as input to Teague's solver for estimating the phase residual,

$$\left.\frac{\mathrm{d}I}{\mathrm{d}z}\right|_{\mathrm{res}} = -\frac{\lambda}{2\pi}\vec{\nabla}\cdot I\vec{\nabla}\phi_{r1}, \tag{10}$$

where ϕ_{r1} is the current estimate of the phase residual [ϕ_{res} in Eq. (7)], after the first iteration. The phase residual estimated is then subtracted from the phase ϕ_{TIE} estimated previously to give an improved phase estimate. Additional iterations can then be used to further refine the result.

To understand how the curl of the Poynting vector couples into the next iteration of Teague's solver, we examine the intensity derivative residual in Eq. (9). Consider the Helmholtz decomposition of the vector field $\vec{\nabla}\psi/I$,

$$\vec{\nabla}\psi/I = \vec{\nabla}\phi_{\mathrm{TIE}} + \vec{\nabla}\times\vec{\mathbf{A}}_2, \tag{11}$$

where the scalar potential is simply ϕ_{TIE} according to Eq. (3), and $\vec{\mathbf{A}}_2$ denotes the vector potential. By substituting Eqs. (2) and (8) into Eq. (9), and considering the relation in Eq. (11), we obtain

$$\left.\frac{\mathrm{d}I}{\mathrm{d}z}\right|_{\mathrm{res}} = -\frac{\lambda}{2\pi}\{\nabla^2\psi_1 - \vec{\nabla}\cdot I\vec{\nabla}\phi_{\mathrm{TIE}}\}, \tag{12}$$

$$\Rightarrow \left.\frac{\mathrm{d}I}{\mathrm{d}z}\right|_{\mathrm{res}} = -\frac{\lambda}{2\pi}\vec{\nabla}\cdot I\vec{\nabla}\times\vec{\mathbf{A}}_2. \tag{13}$$

The curl term $\vec{\nabla}\times\vec{\mathbf{A}}_2$ is thus responsible for the derivative residual on plugging the solved phase back into the TIE. The TIE solution of the residual intensity derivative [Eq. (10)] will try to estimate the error arising due to this curl, which is in fact directly related to the Poynting vector curl $\vec{\nabla}\times\vec{\mathbf{A}}_1$ from Eqs. (5) and (11),

$$\nabla\times\nabla\times\vec{\mathbf{A}}_2 = -\nabla\times\left(\frac{\nabla\times\vec{\mathbf{A}}_1}{I}\right), \tag{14}$$

which holds also for vector potentials of any two successive iterations. In the absence of a curl in the power flow, $\vec{\mathbf{A}}_1 = \vec{\mathbf{A}}_2 = 0$, and hence, the residual intensity derivative vanishes such that the solution converges immediately. In the presence of a curl, however, subsequent iterations will recover some of the curl missed in the previous iteration, the solution reaching convergence when the estimate of the phase gradient at the ith iteration, $\vec{\nabla}\psi_i/I$, approaches zero curl, i.e., $\vec{\mathbf{A}}_{i+1}\to 0$. A more rigorous

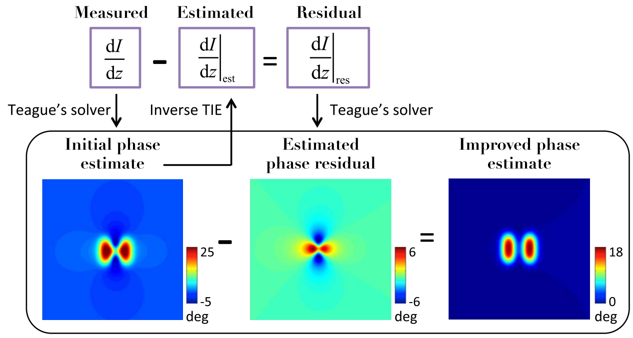

Fig. 3. Simulation showing the first iteration of our algorithm. Teague's solver recovers the initial phase estimate; then we plug that into the TIE to find the estimated intensity derivative. The residual between the measured and estimated intensity derivatives is plugged into Teague's solver a second time in order to estimate the phase residual, which is subtracted from the recovered phase for an improved estimate.

formulation of the convergence criteria would have to include the interplay of the object curl, numerical and focus sampling, and the severity of the curl.

A simulation of the phase residual estimated from the first iteration is shown in Fig. 3. After only one iteration, the improved phase estimate is already very close to the true phase (shown in Fig. 2), with the root mean square (RMS) phase error having dropped by about 42%, from 0.0087 rad/pixel for Teague's solver to 0.005 rad/pixel for our iterative algorithm. Subsequent iterations further improve the estimate of the phase and its residual.

Since the reduction in the error is due to the recovery of the curl, our algorithm also produces an estimate of the curl components, which were previously considered immeasurable. For the simulation case (where the true curl components are known), we plot the error in our curl estimate as iterations progress (see Fig. 4). The plots compare the Poynting vector curl, $\vec{\nabla}\times I\vec{\nabla}\phi = \vec{\nabla}I\times\vec{\nabla}\phi$, for the true object with that recovered by the iterative method. As expected, the error in the curl is progressively reduced, with diminishing gains at each iteration. Notice that the error does not go to 0, since not all of the curl effects were transferred into intensity measurements. However, these unobservable areas of the curl do not produce phase errors in our result. If the goal is to fully measure the curl terms, then a systematic variation of the intensity would be needed [31,32].

4. Experimental Results

Experiments were performed on an AIMS aerial imaging tool at AMTC/Toppan Photomasks at Dresden, Germany. The AIMS tool replicates the projection printing process, with demagnification to allow the wafer plane intensity to be captured by a camera. The experimental parameters and the mask match the simulations described earlier (240 nm square feature on an OMOG mask). Here, we use partially coherent illumination with $\sigma = 0.3$, which has been shown to produce accurate phase results [4], although larger or nonrotationally symmetric

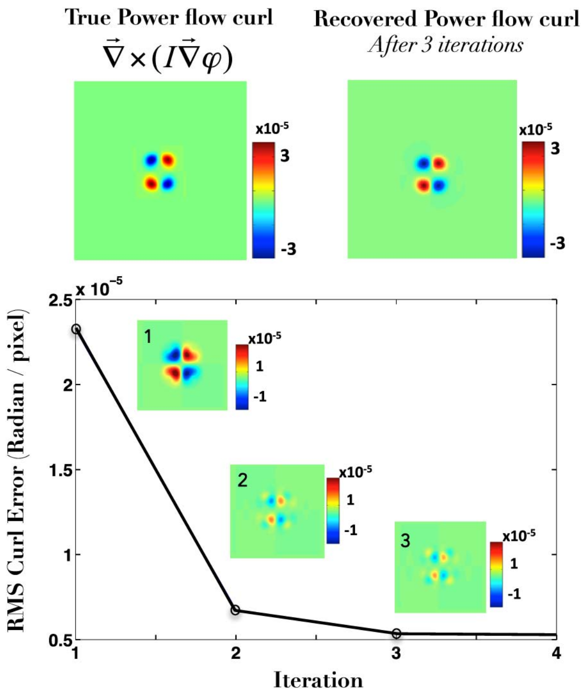

Fig. 4. Estimating curl components with the iterative TIE. The top row shows the true curl for the simulated mask, and the corresponding curl recovered by our iterative algorithm. The bottom plot shows that the RMS error in our estimate of the curl diminishes progressively as the algorithm iterates. Errors in the curl component estimation for the first three iterations of the algorithm are shown as insets.

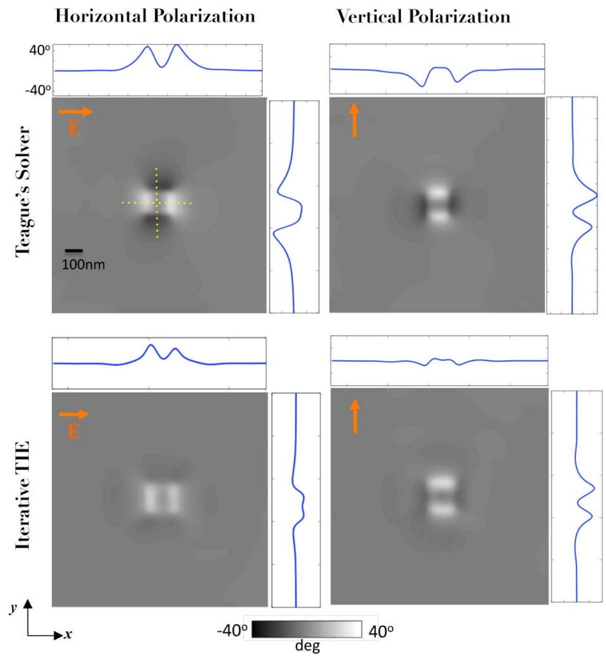

Fig. 5. Experimental results for our iterative TIE method, as compared with those for the traditional Teague's solver, with a 240 nm square feature on an OMOG mask. The top row shows the phase recovered by Teague's solver, with nonphysical saddle artifacts due to the Poynting vector curl at the feature corners. The bottom row shows the phase recovered by the iterative solver, where artifacts have been corrected, clearly showing the presence of phase edges that match well the theoretical predictions. On the left is the result for illumination polarized in the horizontal direction, whereas on the right is that for the vertical direction, showing strong polarization dependence, as expected.

sources [2,33] would require more sophisticated algorithms [34–37]. Images were captured with 10 nm defocus steps across a 200 nm range, building up a through-focus stack. Then, the intensity derivative was calculated using the fitting methods described in [6,14]. Note that although the TIE equation is based on the paraxial approximation, it is justified for the mask-side NA of 0.3375 in the experiments here. More details on the experimental setup can be found in [23].

Images of the experimentally recovered phase are shown in Fig. 5. We clearly observe electromagnetic phase edge effects in all the results. In the experiments, we study two situations, one with horizontally polarized illumination and one with vertically polarized illumination. The phase recovered shows much stronger phase edge effects along the direction perpendicular to the illumination polarization, as predicted by rigorous electromagnetic field simulations [38].

In comparing our iterative algorithm to the traditional TIE method, we see that the phase images recovered by Teague's solver have saddle-shaped artifacts that cause negative phase values. These clearly nonphysical artifacts resemble the error seen in simulation results in the earlier sections, indicating that they are indeed due to the power flow curl near the corners of the square feature. With our iterative solver, however, they are removed and we get a much cleaner picture of the phase edge effects.

The results match well the rigorous simulation-based boundary layer model theory [38], which assumes that the peak phase value of 40 deg in Fig. 5 is a convolution of the 90 deg boundary layer with the point spread function of the system. The smaller phase peaks for the edges parallel to the electric field in Fig. 5 likely indicate that OMOG is similar to attenuating phase shift mask (ATT-PSM), in that the diffraction at the primary edge reduces with the rotation of the polarization and the phase drops in magnitude by about a factor of 5. A detailed analysis can be found in [23].

5. Conclusion

We have demonstrated both theoretically and experimentally an iterative extension to the Transport of Intensity method that provides both accurate phase recovery and an estimate of the Poynting vector curl. Our method is particularly useful for the situation of curl-induced artifacts due to strong absorption, for which we provide a motivating example in lithography. We show that phase edge effects due to 3D electromagnetic interactions break the curl-free assumption of the traditional TIE (Teague's method). However, by employing our iterative TIE solver, we can remove these artifacts and can also solve for curl components in the process. The solution removes curl-induced phase errors with only a few iterations, providing significantly improved results without much computational overhead. Results were demonstrated for a square feature on an OMOG mask, with experimental data being captured in an aerial imaging tool. The method serves to elucidate the influence of power-flow curl on defocus-based phase recovery, and should find general use in many applications, particularly those with strong absorption at the sample.

This work was sponsored by IMPACT+ member companies: Applied Materials, ARM, ASML, Global Foundries, IBM, Intel, KLA-Tencor, Mentor Graphics, Panoramic Tech, Qualcomm, Samsung, SanDisk, and Tokyo Electron. We also thank George Barbastathis, Yunhui Zhu, and Jon Petruccelli for insightful discussions.

References

1. M. R. Teague, "Deterministic phase retrieval: a Green's function solution," J. Opt. Soc. Am. **73**, 1434–1441 (1983).
2. N. Streibl, "Phase imaging by the transport equation of intensity," Opt. Commun. **49**, 6–10 (1984).
3. A. Barty, K. Nugent, D. Paganin, and A. Roberts, "Quantitative optical phase microscopy," Opt. Lett. **23**, 817–819 (1998).
4. E. D. Barone-Nugent, A. Barty, and K. A. Nugent, "Quantitative phase-amplitude microscopy I: optical microscopy," J. Microsc. **206**, 194–203 (2002).
5. C. Zuo, Q. Chen, Y. Yu, and A. Asundi, "Transport-of-intensity phase imaging using Savitzky–Golay differentiation filter-theory and applications," Opt. Express **21**, 5346–5362 (2013).
6. Z. Jingshan, R. A. Claus, J. Dauwels, L. Tian, and L. Waller, "Transport of intensity phase imaging by intensity spectrum fitting of exponentially spaced defocus planes," Opt. Express **22**, 10661–10674 (2014).
7. K. Nugent, T. Gureyev, D. Cookson, D. Paganin, and Z. Barnea, "Quantitative phase imaging using hard x-rays," Phys. Rev. Lett. **77**, 2961–2964 (1996).
8. K. A. Nugent, "X-ray noninterferometric phase imaging: a unified picture," J. Opt. Soc. Am. A **24**, 536–547 (2007).
9. M. Beleggia, M. Schofield, V. Volkov, and Y. Zhu, "On the transport of intensity technique for phase retrieval," Ultramicroscopy **102**, 37–49 (2004).
10. T. C. Petersen, V. J. Keast, and D. M. Paganin, "Quantitative TEM-based phase retrieval of MgO nano-cubes using the transport of intensity equation," Ultramicroscopy **108**, 805–815 (2008).
11. K. Ishizuka and B. Allman, "Phase measurement of atomic resolution image using transport of intensity equation," J. Electron Microsc. **54**, 191–197 (2005).
12. N. Loomis, L. Waller, and G. Barbastathis, "High-speed phase recovery using chromatic transport of intensity computation in graphics processing units," in *Biomedical Optics and 3-D Imaging* (Optical Society of America, 2010), paper JMA7.
13. M. Soto and E. Acosta, "Improved phase imaging from intensity measurements in multiple planes," Appl. Opt. **46**, 7978–7981 (2007).
14. L. Waller, L. Tian, and G. Barbastathis, "Transport of intensity phase-amplitude imaging with higher order intensity derivatives," Opt. Express **18**, 12552–12561 (2010).
15. D. Paganin and K. A. Nugent, "Noninterferometric phase imaging with partially coherent light," Phys. Rev. Lett. **80**, 2586–2589 (1998).
16. T. Gureyev, Y. Nesterets, D. Paganin, A. Pogany, and S. Wilkins, "Linear algorithms for phase retrieval in the Fresnel region. 2. Partially coherent illumination," Opt. Commun. **259**, 569–580 (2006).
17. T. E. Gureyev, A. Roberts, and K. A. Nugent, "Partially coherent fields, the transport-of-intensity equation, and phase uniqueness," J. Opt. Soc. Am. A **12**, 1942–1946 (1995).
18. L. J. Allen, H. M. L. Faulkner, K. A. Nugent, M. P. Oxley, and D. Paganin, "Phase retrieval from images in the presence of first-order vortices," Phys. Rev. E **63**, 037602 (2001).
19. A. Lubk, G. Guzzinati, F. Börrnert, and J. Verbeeck, "Transport of intensity phase retrieval of arbitrary wave fields including vortices," Phys. Rev. Lett. **111**, 173902 (2013).
20. V. Volkov and Y. Zhu, "Lorentz phase microscopy of magnetic materials," Ultramicroscopy **98**, 271–281 (2004).
21. J. A. Schmalz, T. E. Gureyev, D. M. Paganin, and K. M. Pavlov, "Phase retrieval using radiation and matter-wave fields: validity of Teague's method for solution of the transport-of-intensity equation," Phys. Rev. A **84**, 023808 (2011).
22. J. A. Ferrari, G. A. Ayubi, J. L. Flores, and C. D. Perciante, "Transport of intensity equation: validity limits of the usually accepted solution," Opt. Commun. **318**, 133–136 (2014).
23. A. Shanker, M. Sczyrba, B. Connolly, F. Kalk, A. Neureuther, and L. Waller, "Critical assessment of the transport of intensity equation as a phase recovery technique in optical lithography," Proc. SPIE **9052**, 90521D (2014).
24. A. Shanker, L. Waller, and A. R. Neureuther, "Defocus based phase imaging for quantifying electromagnetic edge effects in photomasks," Master's thesis (University of California, 2014).
25. C. Zuo, Q. Chen, L. Huang, and A. Asundi, "Phase discrepancy analysis and compensation for fast Fourier transform based solution of the transport of intensity equation," Opt. Express **22**, 17172–17186 (2014).
26. K. Adam and A. Neureuther, "Simplified models for edge transitions in rigorous mask modeling," Proc. SPIE **4346**, 331–344 (2001).
27. J. Tirapu-Azpiroz, P. Burchard, and E. Yablonovitch, "Boundary layer model to account for thick mask effects in photolithography," Proc. SPIE **5040**, 1611–1619 (2003).
28. J. T. Azpiroz, A. E. Rosenbluth, K. Lai, C. Fonseca, and D. Yang, "Critical impact of mask electromagnetic effects on optical proximity corrections performance for 45 nm and beyond," J. Vac. Sci. Technol. B **25**, 164–168 (2007).
29. T. Gureyev and K. Nugent, "Rapid quantitative phase imaging using the transport of intensity equation," Opt. Commun. **133**, 339–346 (1997).
30. V. Volkov, Y. Zhu, and M. D. Graef, "A new symmetrized solution for phase retrieval using the transport of intensity equation," Micron **33**, 411–416 (2002).
31. A. Shanker, L. Tian, and L. Waller, "Defocus based quantitative phase imaging by coded illumination," Proc. SPIE **8949**, 89490R (2014).
32. Y. Zhu, A. Pan, and G. Barbastathis, "Low-noise TIE phase imaging by structured illumination," in *Computational Optical Sensing and Imaging* (Optical Society of America, 2014), paper CTh3C-5.
33. A. M. Zysk, R. W. Schoonover, P. S. Carney, and M. A. Anastasio, "Transport of intensity and spectrum for partially coherent fields," Opt. Lett. **35**, 2239–2241 (2010).
34. J. C. Petruccelli, L. Tian, and G. Barbastathis, "The Transport of intensity equation for optical path length recovery using partially coherent illumination," Opt. Express **21**, 14430–14441 (2013).
35. Z. Jingshan, L. Tian, R. A. Claus, J. Dauwels, and L. Waller, "Partially coherent phase recovery by Kalman filtering," in *Frontiers in Optics 2013 Postdeadline* (Optical Society of America, 2013), paper FW6A.9.
36. M. H. Jenkins, J. M. Long, and T. K. Gaylord, "Multifilter phase imaging with partially coherent light," Appl. Opt. **53**, D29–D39 (2014).
37. Z. Jingshan, L. Tian, J. Dauwels, and L. Waller, "Partially coherent phase microscopy with arbitrary illumination source shape," in *Computational Optical Sensing and Imaging* (Optical Society of America, 2014), paper CTu1C5.
38. M. Miller, "Mask edge effects in optical lithography and chip level modeling methods," Ph.D. thesis (University of California, 2010).